Self-Consistent Simulation of the Excitation of Compressional Alfvén Eigenmodes and Runaway Electron Diffusion in Tokamak Disruptions

Chang Liu,[1,*] Andrey Lvovskiy,[2] Carlos Paz-Soldan,[3] Stephen C. Jardin,[1] and Amitava Bhattacharjee[1,4]
[1]*Princeton Plasma Physics Laboratory, Princeton, New Jersey 08540, USA*
[2]*General Atomics, San Diego, California 92121, USA*
[3]*Columbia University, New York, New York 10027, USA*
[4]*Princeton University, Princeton, New Jersey 08544, USA*

(Received 13 March 2023; revised 21 May 2023; accepted 19 July 2023; published 24 August 2023; corrected 23 May 2024)

Alfvénic modes in the current quench (CQ) stage of the tokamak disruption have been observed in experiments. In DIII-D the excitation of these modes is associated with the presence of high-energy runaway electrons (REs), and a strong mode excitation is often associated with the failure of RE plateau formation. In this work we present results of self-consistent kinetic-MHD simulations of RE-driven compressional Alfvén eigenmodes (CAEs) in DIII-D disruption scenarios, providing an explanation of the CQ modes. Simulation results reveal that high energy trapped REs can have resonance with the Alfvén mode through their toroidal precession motion, and the resonance frequency is proportional to the energy of REs. The mode frequencies and their relationship with the RE energy are consistent with experimental observations. The perturbed magnetic fields from the modes can lead to spatial diffusion of REs including the nonresonant passing ones, thus providing the theoretical basis for a potential approach for RE mitigation.

DOI: 10.1103/PhysRevLett.131.085102

Tokamak disruption is one of the most important challenges to the success of magnetically confined thermonuclear fusion through tokamaks [1]. High-energy runaway electron (RE) beams can be generated during a disruption event. These electrons can carry a large portion of predisruption magnetic energy through induction electric field acceleration, and cause severe damage to the plasma-facing material in case of localized loss to the wall [2]. A shattered pellet injection system has been introduced in ITER for disruption and RE mitigation, and several complementary mitigation strategies are being actively investigated.

Although high-energy RE beams are dangerous to the operation of tokamaks, they can also provide energy that drives kinetic instabilities, which can lead to energy and spatial diffusion of the REs and suppress their population growth. This idea is supported by disruption experiments in DIII-D [3,4] and ASDEX Upgrade [5], where magnetic field oscillations with frequencies in the MHz ranges have been detected during the current quench phase when an RE beam is present. New diagnostics have suggested that the mode has a dominant polarization of a compressional wave [6]. In DIII-D, it is also observed that the strong excitation of current quench modes is often associated with the failure of RE plateau formation, providing evidence for the dissipation of the RE beam by the Alfvén modes. The excitation of Alfvén waves driven by RE spatial inhomogeneities has been theoretically predicted [7,8]. Compared to the higher frequency whistler wave instabilities [9] observed in the low-density flat-top Ohmic scenarios [10–12], Alfvén modes are less affected by electron-ion collisional damping which is strong in the disruption phase due to the low electron temperature [8].

In this Letter we report the first self-consistent simulation of the excitation of the Alfvén mode driven by high-energy runaway electrons. The kinetic MHD code M3D-C1-K [13] was employed for the simulation, in which REs were treated as kinetic particles and simulated using the particle-in-cell (PIC) method, and their current was coupled into the magnetohydrodynamics (MHD) equations. Similar simulation methods have been used in previous studies for the compressional Alfvén eigenmodes (CAEs) driven by energetic ions [14], and shear Alfvén waves driven by energetic electrons [15]. The electrons are simulated following the gyrokinetic equations including the correction for highly relativistic particles [16], and finite-Larmor-radius (FLR) effects by doing averaging along gyro orbits. Simulation results showed that the modes are driven by high-energy trapped runaway electrons [8], and the excited mode spectrum depends sensitively on the resonance between the mode frequency and the trapped REs precession frequency. It was also verified in the nonlinear simulation that the perturbed magnetic fields of the excited modes can lead to spatial diffusion of REs including the nonresonant ones.

The simulation was set up as follows. A plasma equilibrium constructed using EFIT [30] from DIII-D shot 177028 at $t = 1208$ ms was used, which is 2 ms later than the initial Ar injection triggering the disruption [3].

After the injection, the plasma is mostly composed of electrons and Ar^{2+}. The core electron density is $n_e = 4 \times 10^{20}$ m^{-3} and the electron temperature is around 5 eV. A temperature-dependent Spitzer resistivity is used in the Ohm's law to account for the resistive damping of the mode. The Dirichlet boundary condition is used for the velocity and the perturbed magnetic fields. For runaway electrons, we use a tail distribution with a peak energy and collimated along the magnetic field with finite pitch-angle width. This equilibrium distribution can be written as $f_0 = G(p)H(\xi)$, where $G(p)$ is the distribution of the absolute value of momentum p normalized to $m_e c$ (m_e is the electron mass and c is the speed of light),

$$G(p) = \exp\left[-(p - p_0)^2/\Delta p\right]. \tag{1}$$

The energy distribution is inspired by the kinetic simulation result of hot-tail generation [8], which shows that the remnant of the Maxwellian tail can form a bump-on-tail distribution after thermal quench with a peak (p_0) and finite width (Δp). $H(\xi)$ is the distribution of cosine of RE pitch angle ($\xi = \cos\theta = p_\parallel/p$, $p_\parallel$ is the RE momentum along the local magnetic field) [17],

$$H(\xi) = \frac{A}{2\sinh A}\exp\left[A\xi\right]. \tag{2}$$

Where $A(p) = 2\hat{E}/(1+Z^*)\cdot p^2/\sqrt{p^2+1}$, $\hat{E}$ is the parallel electric field (~3 V/m from experiments) normalized to the relativistic RE critical electric field $E_c = n_e e^3 \log\Lambda/4\pi\epsilon_0^2 m_0 c^2$. The width of the pitch-angle distribution is determined by the balance between the electric field drag and the collisional pitch-angle scattering [18]. Here the value of Z^* is defined by taking into account the partial screening effect of argon, given that the fast electrons can penetrate screening of bounded electrons of partially ionized atoms and get deflected by the nuclei charge [19,20]. It can be estimated following Eq. (5) in [21],

$$Z^* = Z_{\rm eff} + \frac{1}{\ln\Lambda}\frac{n_{\rm Ar}}{n_e}\left[(Z_{\rm Ar}^2 - Z_{\rm eff}^2)\ln(\bar{a}_{\rm Ar}p) - \frac{2}{3}(Z_{\rm Ar} - Z_{\rm eff})^2\right] \tag{3}$$

where $Z_{\rm Ar} = 18$, $Z_{\rm eff} = 2$ and $\bar{a}_{\rm Ar}$ is the effective ion size of Ar^{2+}. For δf simulation, f_0 is then used to calculate the particle weight evolution. Note that in this work we ignore the further acceleration or pitch-angle scattering of the RE beam, assuming that the timescale of these processes is longer compared to that of the mode excitation.

We first conducted linear simulations of CAE excitation using δf method. Figure 1(a) summarizes the dominant AE frequency from linear simulations of $n = 1$ mode using a narrow energy distribution $\Delta p \sim 1.2$ MeV and varying p_0 value. The core RE density is 3×10^{16} m^{-3}. It is found that the frequency of the excited most unstable mode (blue line) follows a staircaselike function with RE energy, and the spacing between adjacent modes is about 0.2–0.4 MHz. The linear growth rates (red line) increase with mode frequency for low RE energy cases, but remain almost constant for high RE energy cases. The mode frequency magnitude and spacing between adjacent eigenmodes are consistent with experiments [3]. However, the highest mode frequency we found is around 1.4 MHz, which is smaller than in the experiment. Each level of the staircase represents a different mode structure in the poloidal plane. The collisional damping rate is calculated by subtracting the linear growth rates from simulations without and with resistivity. It follows a quadratic function of REs, which is consistent with previous analysis [8]. The mode structures of two linear simulations are shown in Figs. 1(b) and 1(c). For all these excited modes, the perturbed magnetic fields satisfy $\delta B_\parallel \gg \delta B_\perp$, indicating that the mode is dominantly a compressional Alfvén eigenmode. Compared to shear Alfvén modes, CAEs are global modes with large radial extent and can have components of multiple poloidal mode numbers. The eigenmode structure observed is consistent with the previous calculation of CAEs by solving the Helmholtz equation [22,23].

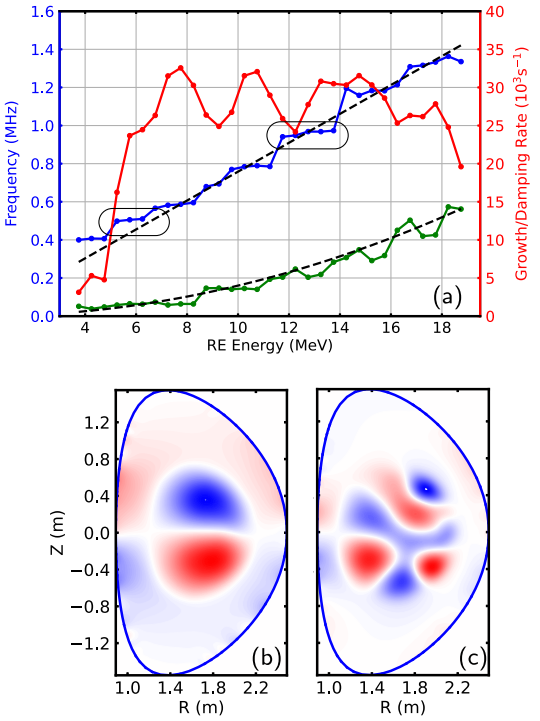

FIG. 1. (a) Frequency (blue line), growth rate (red line), and collisional damping (green line) of dominant CAE from linear simulation using varying RE energy (p_0). The two dashed lines mark the linear and quadratic functions of RE energy. The mode structure ($\delta B_\parallel$) of the two eigenmodes, corresponding to frequencies of 0.50 MHz and 0.93 MHz, are shown in (b) and (c).

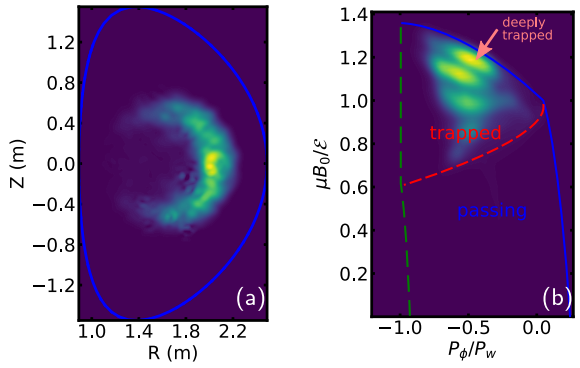

FIG. 2. (a) Distribution of the absolute value of particle weight in the poloidal plane from linear simulation of 0.93 MHz (Fig. 1(c)). (b) Distribution of the absolute value of particle weight in the RE phase space of P_ϕ (toroidal momentum, normalized to the wall magnetic flux P_w) and $\mu B_0/\mathcal{E}$ where μ is the RE magnetic moment and $\mathcal{E}$ is the particle kinetic energy. The boundary between trapped and passing particles is marked as a red dashed line.

To understand the excitation mechanism of CAEs, the perturbed runaway electron distribution is analyzed. The distributions of the absolute value of particle weight in a poloidal plane and in RE phase space for one linear simulation ($\omega = 0.93$ MHz) after the mode gets excited are shown in Fig. 2. It is found that, although the REs are mostly passing electrons, most of the resonant particles with large weight are trapped electrons. This is because these trapped electrons can satisfy the resonance condition with the CAEs. For passing electrons, even considering the relativistic effect, both the cyclotron frequency (~5 GHz) and the transit frequency (~20 MHz) are too large compared to the mode frequency, and only a small population of barely passing electron can satisfy the resonance condition. However, for deeply trapped relativistic REs, the toroidal precession frequency

$$\omega_d = \frac{\gamma c^2}{rR\omega_{ce0}} \tag{4}$$

can satisfy the resonance condition $\omega = n\omega_d$. Here $\omega_{ce0} = eB/m_e$ is the cyclotron frequency of unrelativistic electrons, and R and r are the major and minor radius of the trapped electron orbit. The precession motion is driven by the drift motion of REs due to magnetic field curvature and gradient. Note that unlike the transit frequency which only depends on the electron's velocity, the toroidal precession frequency is proportional to the relativistic factor (γ). This resonance mechanism has been used to explain the excitation of a beta-induced Alfvén eigenmode (BAE) driven by suprathermal electrons without considering the relativistic effect [24]. The resonance condition helps explain the linear relationship between the excited mode frequency and the runaway electron energy shown in Fig. 1(a). Following Eq. (4), it can be estimated that for a deeply trapped relativistic electron with $\gamma = 20$ at an orbit radius of $r = 0.4\,m$, the toroidal precession frequency is 1.2 MHz, which is consistent with results in Fig. 1(a).

For CAEs, most of the electromagnetic perturbation lies in $\delta B_\parallel$ and $\delta E_\perp$. The resonance electrons will be affected by the $\mathbf{E}\times\mathbf{B}$ drifts, the magnetic field gradient drift, and the mirror forces. These forces can lead to a change in the canonical angular momentum, which can cause the trapped particle orbit to shift in the radial direction. This means that a radial gradient of the trapped runaway electrons can provide a drive for the mode, similar to the energetic ion drive for the shear Alfvén mode. Following the derivations in [8], the growth rate of CAEs driven by RE can be estimated as

$$\gamma_L = \frac{4\pi^2 e^2}{\mathcal{E}_{\rm mode}} \int \frac{|\langle G\rangle|^2}{\omega} \delta(\omega - n\omega_d) \times \left[\frac{\omega}{v_\parallel}\left(\frac{\partial}{\partial p_\parallel}\right) + \left(\frac{\omega R}{v_\parallel} - n\right)\left(\frac{\partial}{\partial \psi}\right)\right] f d^3\mathbf{p}, \tag{5}$$

where $\mathcal{E}_{\rm mode}$ is the total energy associated with the mode, $\langle G\rangle$ describes the orbit-averaged energy exchange rate between the particles and the mode, and ψ is the poloidal magnetic flux. The dominant contribution in Eq. (5) comes from the radial gradient of resonant REs ($\partial/\partial\psi$ term). The energy exchange rates associated with both gradient drift ($\delta\mathbf{E}_\perp \cdot \mathbf{v}_d$, where $\mathbf{v}_d$ is the drift velocity) and gyromotion ($\delta\mathbf{E}_\perp \cdot \mathbf{v}_\perp$, where $\mathbf{v}_\perp$ is the perpendicular gyro velocity) are proportional to the resonant RE energy (γ). In addition, the gradient drifts are larger for modes with larger $k_\perp$. Both factors can lead to higher mode growth rates associated with higher RE energy. However, large $k_\perp$ can also lead to more cancellation of energy exchange in the integral along the orbit, and the pitch-angle distribution of higher energy REs is more peaked [Eq. (2)], meaning that the population of trapped REs is smaller. In addition, the collisional damping is stronger for higher frequency modes. These two factors limit the excitation of higher frequency CAEs.

Based on the linear simulation results, we conducted a nonlinear simulation with the $n = 1$ mode only and simulations with multiple toroidal modes enabled using the full-f method. For the $n = 1$ simulation, the nonlinear terms in the PIC simulation are enabled, and the evolution of the RE distribution function will affect the mode saturation. A wider RE distribution in energy space ($p_0 \sim 12$ MeV and $\Delta p \sim 7.5$ MeV) is used. Figure 3 shows the spectrogram of perturbed $\delta B_\parallel$ at the magnetic axis in one poloidal plane from the nonlinear simulation. It is found that multiple discrete modes can be excited and reach comparable amplitudes at saturation [Fig. 3(b)]. In the later stages of the simulation, three dominant modes with frequencies 0.68 MHz, 0.82 MHz, and 0.93 MHz can persist till the end of simulation without significant decay. The excited mode frequencies are almost constant in time without any frequency chirping. We also conducted

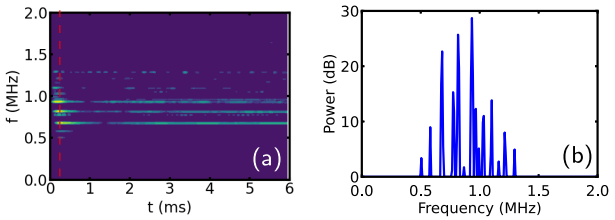

FIG. 3. Spectrogram of excited CAEs from nonlinear simulation with only $n = 1$ (a). The color indicated the mode power in the log scale. The power spectrum at $t = 0.2$ ms (red dashed line) is shown in (b).

a full-torus nonlinear simulation including both the particle nonlinearity and coupling between different MHD modes. However, it is found that the excitation of the $n = 0$ and $n = 2$ components of magnetic perturbations is small in the simulation, indicating that the mode amplitude is not large enough to cause strong mode-mode interactions.

The simulation results are mostly consistent with the experimental observations [3]. In experiments, it is found that the current quench mode can only be excited when RE energy passes a certain threshold, and the low frequency modes are the first to get excited. This is consistent with our linear analysis, as the excited mode frequency depends on the resonant RE energy. Note that in experiments, the hot-tail REs are accelerated to higher energy by the inductive electric field, which has been verified through gamma ray imager (GRI) measurement [3]. Therefore the higher frequency modes will be driven later than the lower frequency ones. According to the kinetic simulation in [8], these multiple excited modes can coexist in the plasma like the nonlinear simulation results in Fig. 3. Experimentally observed down-chirping of CAE frequencies is not observed in the nonlinear simulation, indicating the chirping may be caused by evolution of plasma parameters like ion density or particle ionization and recombination, rather than nonlinear effects. New diagnostics of the experiments [6] reveals that the mode has a dominating compressional polarization, and the toroidal mode number is $n = 1$, which are consistent with the nonlinear simulation. Note that $n = 0$ modes are also identified in the experiments [6], but are absent in the simulations. This may be caused by the inaccuracy of diagnostics, or some other kinetic effects of REs which can also lead to excitement of CAEs but are missing in our current simulation model.

We further investigate the transport of REs affected by the excited CAEs. For nonresonant passing REs, a single mode can only lead to a small deviation of the particle orbit from its unperturbed one. But the overlapping of perturbed fields from multiple CAEs with different frequencies can cause decorrelation between particles and modes, and a random walk of nonresonant passing REs in plasma. Considering that the random walk primarily arises from the gradient drift induced by $\delta B_\parallel$ originating from CAEs, the drift velocity can be estimated as follows:

$$v_d = \frac{\gamma m_e v_\perp^2}{2eB_0} k_\perp \frac{\delta B_\parallel}{B_0}, \tag{6}$$

where $k_\perp \approx m/r$, m is the poloidal mode number and r is the minor radius of the electron orbit. The stepsize can be calculated as $v_d t_p$, where $t_p \approx qR/mc$, q is the local safety factor at r, and qR gives an estimate of the connection length of the flux surface. The decorrelation time is $1/\Delta f$ (Δf is the gap CAE frequency between different modes). Combining all these parameters, the diffusion time can be roughly estimated as

$$T_{\text{diff}} \approx \frac{r^2}{(v_d t_p)^2} \frac{1}{\Delta f} \approx \left(\frac{r}{qR}\right)^2 \left(\frac{2eB_0 rc}{\gamma m_e v_\perp^2}\right)^2 \left(\frac{B_0}{\delta B_\parallel}\right)^2 \frac{1}{\Delta f}. \tag{7}$$

For electrons with $\gamma = 24$, $v_\perp^2/c^2 = 0.16$ at orbit $r = 0.3$ m, assuming $B_0 = 2$ T and $\Delta f = 1.0$ MHz, in order to reach a diffusion time around 10 ms, the required value of $\delta B_\parallel$ is around 0.65 T. This value is larger compared to that in the nonlinear simulation. In addition to the gradient drift, additional diffusion can be driven by the parallel streaming associated with the $\delta B_\perp$ field of the mode, and the $\mathbf{E} \times \mathbf{B}$ drift.

In order to test the RE diffusion, we rerun the full-f nonlinear simulation starting from the point when multiple CAEs are excited ($t = 0.2$ ms), and artificially amplify the value of mode δB to check the impact on RE diffusion. The results of the RE diffusion time are summarized in Fig. 4(a). The diffusion time is estimated by calculating the decaying rate of the RE population inside the $r = 0.3$ m flux surface. An example of RE profile diffusion is shown in Fig. 4(b). It is found that although REs in most of the region diffuse to the edge, the RE density near the magnetic axis increases. This may be caused by the fact that diffusion near the axis is small, making it a stagnation point for REs. The obtained diffusion time follows a scaling law of $\delta B_\parallel^{-2}$ which is consistent with the estimation, and the value is an order of magnitude smaller compared to the result in

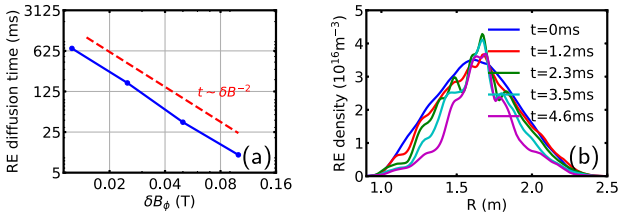

FIG. 4. (a) RE diffusion time vs δB_ϕ of CAEs, from nonlinear simulation with artificially amplified δB. The red dashed line showed the scaling law of $t \sim \delta B_\phi^{-2}$. (b) An example of the RE density profile diffusion process captured after increasing the value of δB_ϕ to 0.05 T.

Eq. (7). However, according to the current simulation results, to reach such a high amplitude of $\delta B_{\parallel}$, the population of high-energy trapped REs must be increase by a minimum factor of 5 from the current setup, which requires other pitch-angle scattering mechanisms than collisions.

In summary, in this Letter we showed a self-consistent model to explain the current quench mode observed in DIII-D and other tokamaks, through kinetic MHD simulation with REs. The excited modes are dominantly CAEs, which can have resonance with trapped REs. The simulation results are mostly consistent with experimental observations, including the structure of the mode frequency spectrum, and mode polarization, and the relationship between the excited mode frequency and the RE energy. The amplitude of the excited modes from our simulation, however, is not large enough to drive significant loss of nonresonant passing REs, which, however, has been observed in experiments.

The excitation of CAEs depends on the presence of trapped REs. In our current model, these trapped REs are generated from collisional pitch-angle scattering. Even though the partial screening effect of high-Z impurities like argon is taken into account, the population of trapped REs is still very small compared to the passing ones. It is possible that other pitch-angle scattering mechanisms may also play important roles in the current quench phase, which can provide additional sources of trapped REs. These mechanisms include the secondary generation due to large-angle scattering [25], scattering effect from higher frequency modes like whistler waves and high-frequency CAEs [26], and scattering from turbulence fields [27]. The diffusion of REs driven by perturbed fields from CAEs is confirmed in the simulation, which shows the potential of this alternative RE mitigation strategy. Furthermore, the present findings highlight the possibility of mitigating RE beams by employing external coils to launch compressional waves, as previously explored in [28].

For other future research, our plan is to expand the current simulation model to incorporate additional physical effects. This involves expanding the nonlinear full-f simulation to encompass the time evolution of the equilibrium RE distribution due to electric force acceleration, collisional dissipation, synchrotron radiation, and RE avalanche. The electric field utilized in the current simulation (approximately 3 V/m) is measured from the plasma edge, and the values remain uncertain for the core region. If the core electric field is much higher, the RE generation may be primarily driven by the avalanche effect rather than hot-tail generation, resulting in a different distribution function shape. The avalanche process can also contribute to the generation of REs with large pitch angles and serve as a source for trapped REs when combined with pitch-angle scattering. While the radial profile of REs in our present simulations is estimated based on the plasma current profile, it can be more accurately modeled by employing other RE kinetic simulation tools like DREAM [29]. Furthermore, in future MHD simulations, we aim to incorporate the shrinkage of the last closed flux surface (LCFS) and examine its impact on the frequency spectrum of CAEs. Additionally, we plan to investigate the transition from CAEs to whistler waves by enabling two-fluid terms in our MHD simulations.

The data that support the findings of this study are openly available at the following [31].

Chang Liu would like to thank Elena Belova, Nikolai Gorelenkov, and Neal Croker for fruitful discussions. This work was supported by the Simulation Center of Runaway Electrons Avoidance and Mitigation (SCREAM) SciDAC center by the Office of Fusion Energy Science and Office of Advanced Scientific Computing of the U.S. Department of Energy, under Contracts No. DE-SC0016268 and No. DE-AC02-09CH11466. This work is also supported by the U.S. Department of Energy, Office of Science, Office of Fusion Energy Sciences, using the DIII-D National Fusion Facility, a DOE Office of Science user facility, under Award No. DE-FC02-04ER54698. This research used the high-performance computing cluster at Princeton University, the computational resources of the National Energy Research Scientific Computing Center (NERSC) under Contract No. DE-AC02-05CH11231, and computational resources of the Oak Ridge Leadership Computing Facility (OLCF) under Contract No. DEAC05-00OR22725.

*cliu@pppl.gov

[1] M. Lehnen *et al.*, Disruptions in ITER and strategies for their control and mitigation, J. Nucl. Mater. **463**, 39 (2015).
[2] A. H. Boozer, Pivotal issues on relativistic electrons in ITER, Nucl. Fusion **58**, 036006 (2018).
[3] A. Lvovskiy, C. Paz-Soldan, N. W. Eidietis, A. D. Molin, X. D. Du, L. Giacomelli, J. L. Herfindal, E. M. Hollmann, L Martinelli, R. A. Moyer, M. Nocente, D. Rigamonti, D. Shiraki, M. Tardocchi, and K. E. Thome, The role of kinetic instabilities in formation of the runaway electron current after argon injection in DIII-D, Plasma Phys. Controlled Fusion **60**, 124003 (2018).
[4] A. Lvovskiy, W. W. Heidbrink, C. Paz-Soldan, D. A. Spong, A. D. Molin, N. W. Eidietis, M. Nocente, D. Shiraki, and K. E. Thome, Observation of rapid frequency chirping instabilities driven by runaway electrons in a tokamak, Nucl. Fusion **59**, 124004 (2019).
[5] P. Heinrich, Investigations of Alfvénic activity during the current quench in ASDEX upgrade, Master Thesis, Technische Universität München (2021).
[6] A. Lvovskiy, C. Paz-Soldan, N. W. Eidietis, A. Dal Molin, G. DeGrandchamp, E. M. Hollmann, J. Lestz, C. Liu, M. Nocente, D. Shiraki, and X. Du, Parametric study of Alfvénic instabilities driven by runaway electrons during the current quench in DIII-D, Nucl. Fusion **63**, 046011 (2023).

[7] T. Fülöp and S. Newton, Alfvénic instabilities driven by runaways in fusion plasmas, Phys. Plasmas **21**, 080702 (2014).
[8] C. Liu, D. P. Brennan, A. Lvovskiy, C. Paz-Soldan, E. D. Fredrickson, and A. Bhattacharjee, Compressional Alfvén eigenmodes excited by runaway electrons, Nucl. Fusion **61**, 036011 (2021).
[9] T. Fülöp, G. Pokol, P. Helander, and M. Lisak, Destabilization of magnetosonic-whistler waves by a relativistic runaway beam, Phys. Plasmas **13**, 062506 (2006).
[10] C. Paz-Soldan, C. M. Cooper, P. Aleynikov, D. C. Pace, N. W. Eidietis, D. P. Brennan, R. S. Granetz, E. M. Hollmann, C. Liu, A. Lvovskiy, R. A. Moyer, and D. Shiraki, Spatiotemporal Evolution of Runaway Electron Momentum Distributions in Tokamaks, Phys. Rev. Lett. **118**, 255002 (2017).
[11] D. A. Spong, W. W. Heidbrink, C. Paz-Soldan, X. D. Du, K. E. Thome, M. A. Van Zeeland, C. Collins, A. Lvovskiy, R. A. Moyer, M. E. Austin, D. P. Brennan, C. Liu, E. F. Jaeger, and C. Lau, First Direct Observation of Runaway-Electron-Driven Whistler Waves in Tokamaks, Phys. Rev. Lett. **120**, 155002 (2018).
[12] C. Liu, E. Hirvijoki, G.-Y. Fu, D. P. Brennan, A. Bhattacharjee, and C. Paz-Soldan, Role of Kinetic Instability in Runaway-Electron Avalanches and Elevated Critical Electric Fields, Phys. Rev. Lett. **120**, 265001 (2018).
[13] C. Liu, S. C. Jardin, H. Qin, J. Xiao, N. M. Ferraro, and J. Breslau, Hybrid simulation of energetic particles interacting with magnetohydrodynamics using a slow manifold algorithm and GPU acceleration, Comput. Phys. Commun. **275**, 108313 (2022).
[14] E. V. Belova, N. N. Gorelenkov, N. A. Crocker, J. B. Lestz, E. D. Fredrickson, S. Tang, and K. Tritz, Nonlinear simulations of beam-driven compressional Alfvén eigenmodes in NSTX, Phys. Plasmas **24**, 042505 (2017).
[15] J. Wang, Y. Todo, H. Wang, and Z.-X. Wang, Simulation of Alfvén eigenmodes destabilized by energetic electrons in tokamak plasmas, Nucl. Fusion **60**, 112012 (2020).
[16] C. Liu, H. Qin, E. Hirvijoki, Y. Wang, and J. Liu, Conservative magnetic moment of runaway electrons and collisionless pitch-angle scattering, Nucl. Fusion **58**, 106018 (2018).
[30] L. L. Lao, J. R. Ferron, R. J. Groebner, W. Howl, H. St. John, E. J. Strait, and T. S. Taylor, Equilibrium analysis of current profiles in tokamaks., Nucl. Fusion **30**, 1035 (1990).
[17] P. Aleynikov and B. N. Breizman, Theory of Two Threshold Fields for Relativistic Runaway Electrons, Phys. Rev. Lett. **114**, 155001 (2015).
[18] P. Aleynikov and B. Breizman, Stability analysis of runaway-driven waves in a tokamak, Nucl. Fusion **55**, 043014 (2015).
[19] L. Hesslow, O. Embréus, A. Stahl, T. C. DuBois, G. Papp, S. L. Newton, and T. Fülöp, Effect of Partially Screened Nuclei on Fast-Electron Dynamics, Phys. Rev. Lett. **118**, 255001 (2017).
[20] B. N. Breizman, P. Aleynikov, E. M. Hollmann, and M. Lehnen, Physics of runaway electrons in tokamaks, Nucl. Fusion **59**, 083001 (2019).
[21] L. Hesslow, O. Embréus, G. J. Wilkie, G. Papp, and T. Fülöp, Effect of partially ionized impurities and radiation on the effective critical electric field for runaway generation, Plasma Phys. Controlled Fusion **60**, 074010 (2018).
[22] E. D. Fredrickson, N. N. Gorelenkov, M. Podesta, A. Bortolon, N. A. Crocker, S. P. Gerhardt, R. E. Bell, A. Diallo, B. LeBlanc, F. M. Levinton, and H. Yuh, Non-linear modulation of short wavelength compressional Alfvén eigenmodes, Phys. Plasmas **20**, 042112 (2013).
[23] H. M. Smith and E. D. Fredrickson, Compressional Alfvén eigenmodes in rotating spherical tokamak plasmas, Plasma Phys. Controlled Fusion **59**, 035007 (2017).
[24] W. Chen *et al.* (HL-2A Team), β-Induced Alfvén Eigenmodes Destabilized by Energetic Electrons in a Tokamak Plasma, Phys. Rev. Lett. **105**, 185004 (2010).
[25] C. J. McDevitt, Z. Guo, and X.-Z. Tang, Avalanche mechanism for runaway electron amplification in a tokamak plasma, Plasma Phys. Controlled Fusion **61**, 054008 (2019).
[26] B. N. Breizman and D. I. Kiramov, Marginal stability constraint on runaway electron distribution, Phys. Plasmas **30**, 022301 (2023).
[27] J. R. Martín-Solís, R. Sánchez, and B. Esposito, Effect of magnetic and electrostatic fluctuations on the runaway electron dynamics in tokamak plasmas, Phys. Plasmas **6**, 3925 (1999).
[28] Z. Guo, C. J. McDevitt, and X.-Z. Tang, Control of runaway electron energy using externally injected whistler waves, Phys. Plasmas **25**, 032504 (2018).
[29] M. Hoppe, O. Embreus, and T. Fülöp, DREAM: A fluid-kinetic framework for tokamak disruption runaway electron simulations, Comput. Phys. Commun. **268**, 108098 (2021).
[31] C. Liu, A. Lvovskiy, C. Paz-Soldan, S. Jardin, and A. Bhattacharjee, Self-consistent simulation of compressional Alfvén eigenmodes excitation and runaway electron diffusion in tokamak disruptions (Princeton Plasma Physics Laboratory, Princeton University, 2023), http://arks.princeton.edu/ark:/88435/dsp01x059cb607.

Correction: Support information in the Acknowledgements section was incomplete and has been fixed.